Applied Physics Letters

RESEARCH ARTICLE | OCTOBER 23 2023

Thermal control of polarization of light with nonlocal plasmonic anisotropic metamaterials

Jingyi Wu ; Anton Yu. Bykov ; Alexey V. Krasavin ; Mazhar E. Nasir ; Anatoly V. Zayats

Appl. Phys. Lett. 123, 171701 (2023)
https://doi.org/10.1063/5.0171298

Applied Physics Letters ARTICLE pubs.aip.org/aip/apl

Thermal control of polarization of light with nonlocal plasmonic anisotropic metamaterials

Cite as: Appl. Phys. Lett. **123**, 171701 (2023); doi: 10.1063/5.0171298
Submitted: 8 August 2023 · Accepted: 21 September 2023 ·
Published Online: 23 October 2023

Jingyi Wu,[a] Anton Yu. Bykov, Alexey V. Krasavin, Mazhar E. Nasir, and Anatoly V. Zayats

AFFILIATIONS

Department of Physics and London Centre for Nanotechnology, King's College London, Strand, London WC2R 2LS, United Kingdom

[a]Author to whom correspondence should be addressed: jingyi.2.wu@kcl.ac.uk

ABSTRACT

Plasmonic nanostructures have demonstrated significant potential for engineering the intensity and polarization state of light with further opportunities to actively manipulate them by external stimulation using nonlinear effects. Plasmonic metamaterials composed of arrays of vertically oriented metallic nanorods have shown a dynamically tunable optical response based on the change of the electron temperature. The modulation of the optical properties is particularly pronounced in the epsilon-near-zero regime and can be further enhanced by nonlocal effects. Here, we experimentally study the optical properties of gold nanorod metamaterials with a strong nonlocal response under optically-induced heating, exploiting temperature dependence of the metal permittivity. Recovering the Stokes parameters of light transmitted through the metamaterial, we demonstrate the change in the polarization of the transmitted light by more than 20% for temperature changes under hundred degrees. Combined with a numerical analysis, this shows the possibility of controlling transmission and polarization state of light by using metamaterial-assisted thermal modulation.

Plasmonic metamaterials, offering readily engineered optical properties, have led to numerous advances in photonics, which include the realization of negative refractive index,[1] fluorescence enhancement,[2] subwavelength imaging,[3] and nanoscale sensing.[4] Self-assembly methods play a crucial role in the realization of optical metamaterials over large scales at low cost. One of such metamaterials produced by a self-assembly technique is formed by an array of vertically oriented metallic nanorods, which diameter, length, and spacing can be easily controlled at the fabrication stage. It has found applications in many areas,[5,6] such as all-optical control of light,[5–10] fluorescence management,[11,12] nonlinear harmonic generation,[12–14] neuromorphic computing,[6,13] microscopy,[15] nanoscale chemistry,[16] quantum photonics,[17] imaging,[18] and sensing.[19]

Optical properties of the plasmonic nanorod material feature extremely strong uniaxial anisotropy, offering an intriguing possibility of having opposite signs of the real parts of effective dielectric permittivity along the principal axes, which results in hyperbolic dispersion. Furthermore, such metamaterial possesses nanostructuring-induced nonlocality (spatial dispersion).[20–23] It is particularly important in the spectral range where the permittivity is close to zero [the so-called epsilon-near-zero (ENZ) regime].[23] At these wavelengths, the optical response of the nanorod metamaterial is very sensitive to the changes of the optical properties of the constituting materials. This property has been used to achieve modulation of light transmitted through the metamaterial using ultrafast changes of the conduction electron energy distribution in the metal,[7] or much slower modulation by thermal means,[24] related to the changes in the electron–phonon scattering.

Very strong uniaxial anisotropy of the metamaterial and the pronounced contrast in modulation of the permittivity components, enhanced by the ENZ effect, made it possible to achieve drastic changes of the polarization of the transmitted light using nonlinearity based on the change of the electron temperature.[25,26] In this work, we exploit the thermal effects on the metamaterial anisotropy to control and modulate the polarization state of the transmitted light and show that such modulation is strongly enhanced in the metamaterial with a nonlocal response. Particularly, in addition to the electron temperature effect, the optically-induced rise of the lattice temperature influences the metal permittivity, therefore, changing the metamaterial anisotropy. The experimental results are further supported by numerical simulations, which take into account temperature-dependent interband and intraband electronic transitions. The observed temperature sensitivity of polarized light transmission through a nonlocal metamaterial may find applications in precise

tuning of the polarization state of light, temperature sensing by optical means, and anticounterfeiting applications.

Gold nanorod metamaterial used in this work was fabricated using electrodeposition of gold into a porous alumina oxide (AAO) matrix obtained by anodization of an Al film[27–30] (Fig. 1). The average geometrical parameters of the nanorod array were obtained from scanning electron microscope (SEM) images: nanorod radius $r = 28$ nm, length $h = 310$ nm, and separation $p = 100$ nm. The metamaterial was formed on a Au (10 nm)/Ta_2O_5 (10 nm)/SiO_2 substrate and annealed at 300 °C for 2 h in order to reduce losses in the electrodeposited metal and, therefore, access pronounced nonlocal optical response by increasing the electron mean free path.[20,21]

Extinction spectra measured at oblique incidence exhibit two typical peaks. The short-wavelength peak, observed at both polarizations of illumination [Fig. 1(a)], originates from transverse dipolar plasmonic resonances of the nanorods, spectrally shifted due to their coupling. The long wavelength peak, observed only with *p*-polarized light, having an electric field component along the nanorods, marks the ENZ region, where the metamaterial becomes opaque.[20] The transverse plasmonic resonance keeps its position with the increase in the incidence angle, while the ENZ peak experiences a clear blue shift with the increase in the incident angle—the behavior related to the impact of nonlocality on the metamaterial optical properties.[20]

The properties of nanorod metamaterial can be described with a use of effective medium theories (EMTs), presenting its effective permittivity in a form of a diagonal tensor, $\varepsilon = [\varepsilon_{xx}, \varepsilon_{yy}, \varepsilon_{zz}]$ with $\varepsilon_{xx} = \varepsilon_{yy}$. At the same time, nanostructuring-induced nonlocal effects cannot be described with a conventional local EMT, and full-vectorial modeling of the exact metamaterial structure is required.[20] Such numerical simulations were performed using a finite element method (COMSOL Multiphysics software). Considering the periodicity of the hexagonal array of nanorods, a unit cell was modeled with Floquet periodic boundary conditions featuring the phase difference linked to the angle of the incident light set on the side boundaries. At the top

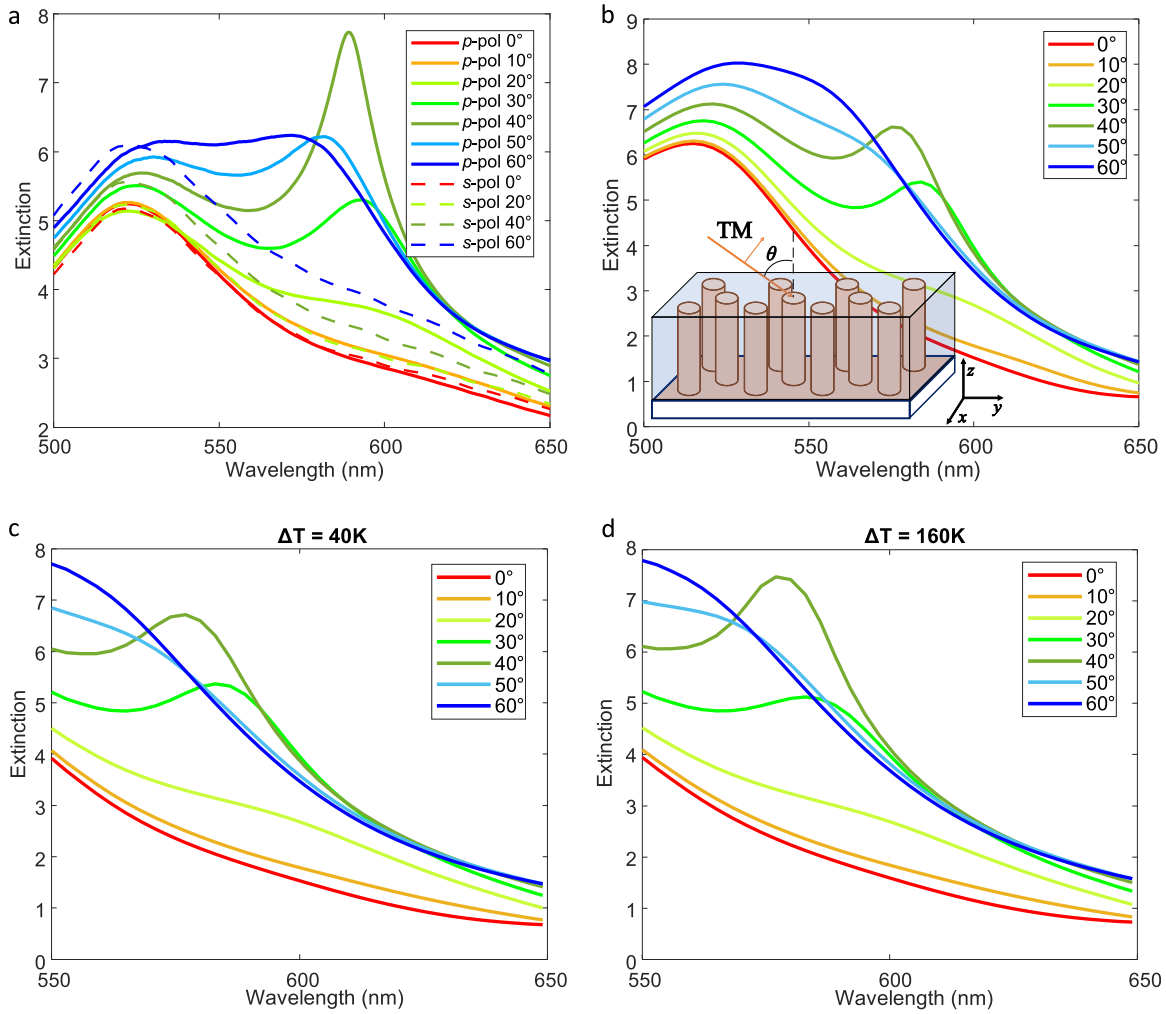

FIG. 1. (a) Extinction spectra of the metamaterial measured with *p*- and *s*-polarized light at various angles of incidence. The metamaterials parameters are $r = 28$ nm, $h = 310$ nm, and $p = 100$ nm. (b) Extinction spectra of the metamaterial simulated using a finite-element method. The inset shows the schematics of the metamaterial. (c) and (d) Numerically simulated extinction spectra at various angles of incidence at elevated temperatures indicated in the panels.

and the bottom of the simulation domain, perfectly matched layers were introduced to assure the absence of backreflection. Optical properties of Al_2O_3, Ta_2O_5, and SiO_2 were taken from Refs. 31–33, respectively. The permittivity of electrodeposited gold was corrected to include scattering on the boundaries of 10 nm grains of the polycrystalline structure using a theoretical approach from Ref. 34. For modeling of the temperature effects, the permittivity of the nanorods and the underlying gold layer was considered to be temperature dependent, while refractive indexes of AAO and silica glass were treated as temperature independent. Numerically simulated extinction spectra agree reasonably well with the experimental observations confirming the nonlocal behavior [cf. Figs. 1(a) and 1(b)]. Slight differences in the amplitude of the extinction peaks can be related to the mismatch between the idealized model of a hexagonal array and the real experimental samples.

The transmission through the metamaterial layer was further numerically studied at elevated temperatures [Figs. 1(c) and 1(d)] with temperature-dependent dielectric permittivity of gold determined using an analytical theory,[35,36] taking into account both the change in the Fermi–Dirac distribution of the free-electron gas affecting the interband absorption and the modification of electron–electron and electron–phonon scattering rates additionally affecting the intraband Drude response.

Specifically, the optical properties of gold at various electron temperatures T_e were calculated using the following approach. The gold permittivity can be decomposed into the contribution defined by interband transitions between occupied *d*-band states and unoccupied states in a hybridized *sp*-band [$\varepsilon^{\text{inter}}(\omega, T_e, T_{ph})$] and the intraband contribution of the conduction electrons in the *sp*-band [$\varepsilon^{\text{intra}}(\omega, T_e, T_{ph})$],

$$\varepsilon_{Au}(\omega, T_e, T_{ph}) = \varepsilon^{\text{inter}}(\omega, T_e, T_{ph}) + \varepsilon^{\text{intra}}(\omega, T_e, T_{ph}). \quad (1)$$

In the visible spectral range, the interband permittivity of gold is defined by three optical transitions, one near the *X* point, and two near the *L* point (L_4^+ and L_{5+6}^+).[37] The imaginary part of the permittivity related to these transitions can be calculated as[35,36]

$$\Im\mathfrak{m}\left[\varepsilon^{\text{inter}}(\omega, T_e, T_{ph})\right] = \frac{A_X J_X(\omega, T_e, T_{ph}) + A_{L_4^+} J_{L_4^+}(\omega, T_e, T_{ph}) + A_{L_{5+6}^+} J_{L_{5+6}^+}(\omega, T_e, T_{ph})}{\hbar\omega^2}, \quad (2)$$

where

$$J_j(\omega, T_e, T_{ph}) = \int_{E_{\min}^j}^{E_{\max}^j} \int D_j(\omega', E)\left(f_l(E - \hbar\omega', T_e) - f_u(E, T_e)\right) B(\omega' - \omega, E, T_e, T_{ph})\, d\omega' dE \quad (3)$$

is the joint density of states (JDOS) for the corresponding transitions with $j = X, L_4^+, L_{5+6}^+$. It is obtained by integration of the JDOS energy distribution $D_j(\omega', E)$ over the excited states in the conduction band with an energy E taking into account Fermi–Dirac distributions $f_l(E, T_e)$ and $f_u(E, T_e)$ of the carriers in the lower (l) and upper (u) bands, respectively, defined by their temperature and playing the leading role in the temperature dependence of the permittivity, and energy- and temperature-dependent broadening of the upper (*sp*-band) due to electron scattering:

$$B(\omega' - \omega, E, T_e, T_{ph}) = \frac{1.76}{2b\gamma^{\text{inter}}(E, T_e, T_{ph})} \cdot \cosh^{-2}\left(\frac{1.76(\omega' - \omega)}{b\gamma^{\text{inter}}(E, T_e, T_{ph})}\right), \quad (4)$$

which is similar to Lorentzian, but with exponential tails presenting a better approximation of the transition line shape in the considered wavelength range.[37,38] The total electron scattering rate,

$$\gamma^{\text{inter}}(E, T_e, T_{ph}) = \gamma_{e-ph}(T_{ph}) + \gamma_{e-e}^E(E, T_e), \quad (5)$$

has two contributions. One $\gamma_{e-ph}(T_{ph})$ is related to electron–phonon scattering:[39]

$$\gamma_{e-ph}(T_{ph}) = \gamma_{e-ph}(T_r) \cdot \frac{2/5 + 4(T_{ph}/T_D)^5 \int_0^{T_D/T_{ph}} \frac{z^4}{\exp(z) - 1} dz}{2/5 + 4(T_r/T_D)^5 \int_0^{T_D/T_r} \frac{z^4}{\exp(z) - 1} dz}, \quad (6)$$

where $T_r = 300$ K and $T_D = 170$ K are the room and Debye temperatures, respectively, and $\gamma_{e-ph}(T_r) = v_F/\Lambda(T_r)$ is the electron–phonon scattering rate at room temperature T_r with v_F being the Fermi velocity and $\Lambda(T_r) = 37.7$ nm being the phonon scattering related electron mean free path at T_r.[40] The other term $\gamma_{e-e}^E(E, T_e)$ is related to energy-dependent electron–electron scattering

$$\gamma_{e-e}^E(E, T_e) = 2K \frac{(k_B T_e)^2 + \left((E - E_F)/\pi\right)^2}{1 + \exp\left(-(E - E_F)/(k_B T_e)\right)}, \quad (7)$$

where E_F is the Fermi energy, k_B is Boltzmann constant, and the value of K was adjusted to match the corresponding temperature dependence for frequency-dependent scattering [see Eq. (8)]. The interband transition coefficients $A_X/A_{L_4^+} = 1$ and $A_X/A_{L_{5+6}^+} = 0.4$, related to the values of the corresponding transition dipole moments, and broadening coefficient $b = 2.5$ were set to fit the Johnson–Cristy data for the permittivity of gold at room temperature.[37,38,41,42]

The real part of the interband permittivity $\Re\mathfrak{e}\left[\varepsilon^{\text{inter}}(\omega, T_e, T_{ph})\right]$ was found from its imaginary part $\Im\mathfrak{m}\left[\varepsilon^{\text{inter}}(\omega, T_e, T_{ph})\right]$ using the Kramers–Kronig relations and an approach based on the Hilbert transform described in Ref. 43. The intraband component of the permittivity is given by the Drude formula

$$\varepsilon^{\text{intra}}(\omega, T_e, T_{ph}) = \varepsilon_{\text{inf}} - \frac{\omega_p^2}{\omega^2 + i\omega\gamma^{\text{intra}}(\hbar\omega, T_e, T_{ph})}, \quad (8)$$

where $\varepsilon_{\text{inf}} = 2$ was set to fit the Johnson–Cristy data for the permittivity of gold at room temperature[41] and $\omega_p = 9.02$ eV is the gold plasma frequency. The electron scattering rate in this case is given by the same expression as in Eq. (5), but with the second term given by the dynamic frequency-dependent electron–electron scattering rate,

$$\gamma_{e-e}^{\omega}(\omega, T_e) = K\left((k_B T_e)^2 + (\hbar\omega/2\pi)^2\right), \quad (9)$$

where $K = 0.3\ \text{eV}^{-2}\,\text{fs}^{-1}$.[44,45]

The simulated extinction spectra for various global temperatures of the metamaterial (at the long considered timescales the electrons and lattice are in thermal equilibrium and, therefore, have the same

temperatures $T_e = T_{ph}$) show distinct blue shifts with the increase in the incident angle, which is indicative of the metamaterial nonlocality, while a clear increase in the amplitude of the ENZ extinction peak with the increase in the temperature is observed at large incidence angles [Figs. 1(c) and 1(d)].

To experimentally investigate the temperature-induced effects on optical properties of the metamaterial, the metamaterial was illuminated at 40° by 532 nm light from a CW laser (Laserglow LLS 0532), which provides heating of the system upon light absorption [Fig. 2(a)]. The diameter of the laser spot was around 5 mm, so the laser illuminates most of the nanostructured area to avoid mechanical stress caused by uneven heating. Broadband light from a halogen lamp was used as probe. Reference optical beam lines for both probe and pump signals were implemented in the measurement setup to monitor their powers and take into account intensity fluctuations. A half-waveplate was placed in front of the spectrometer to compensate for different sensitivities of the spectrometer to different polarizations of the incident light. While light is absorbed primarily in the nanorods, thermal conductance of AAO and glass substrate ensures fast thermal equilibrium established across the metamaterial. Before each measurement at a given control power, the metamaterial was kept under the studied heating conditions for 10 min in order to stabilize its temperature. The temperature was estimated using a thermocouple placed at the edge of the beam on the substrate side of the sample to avoid direct heating by the illuminating beam. The temperature drop across the substrate (∼10 K) was estimated using a known thermal conductivity of glass. To characterize the polarization state of the transmitted probe light, Stokes parameters were monitored employing a conventional measurement method with the use of a polarizer and a quarter-waveplate. To increase the accuracy, the Stokes parameters at every temperature were averaged over ten separate measurements.

The spectral dependence of the Stokes parameters for various powers of the pump light is presented in Fig. 2(b). One can see that around the ENZ wavelength, the Stokes parameters experience drastic changes, also showing the modulation with the increase in the heating laser power (i.e., the temperature of the sample). For example, at the 582 nm wavelength, the Stokes parameters S_1 and S_2 experience temperature-induced changes of ∼0.15 and ∼0.25, respectively. These two parameters determine the orientation angle of the polarization ellipse. Generally, the nature of this temperature dependence can be qualitatively understood in the effective medium approximation, considering the temperature-induced change in the permittivity of the nanorods, which affects differently the $\varepsilon_{xx,yy}$ and ε_{zz} components of the effective permittivity tensor of the metamaterial and, thus, ordinary and extraordinary waves propagating through it. The modulation of S_1 and S_2 over several cycles of the measurement shows the stability of the observed effect [Fig. 2(c)]. In order to visualize the changes in the polarization of the transmitted light better, the corresponding polarization ellipses were recovered from the measured Stokes parameters (Fig. 3). The polarization ellipses of transmitted light rotate in an anticlockwise direction as the temperature increases. Numerical simulations confirm the observed experimental trends, reproducing a temperature-induced rotation of the polarization ellipses [Fig. 3(b)]. The modeling supports the

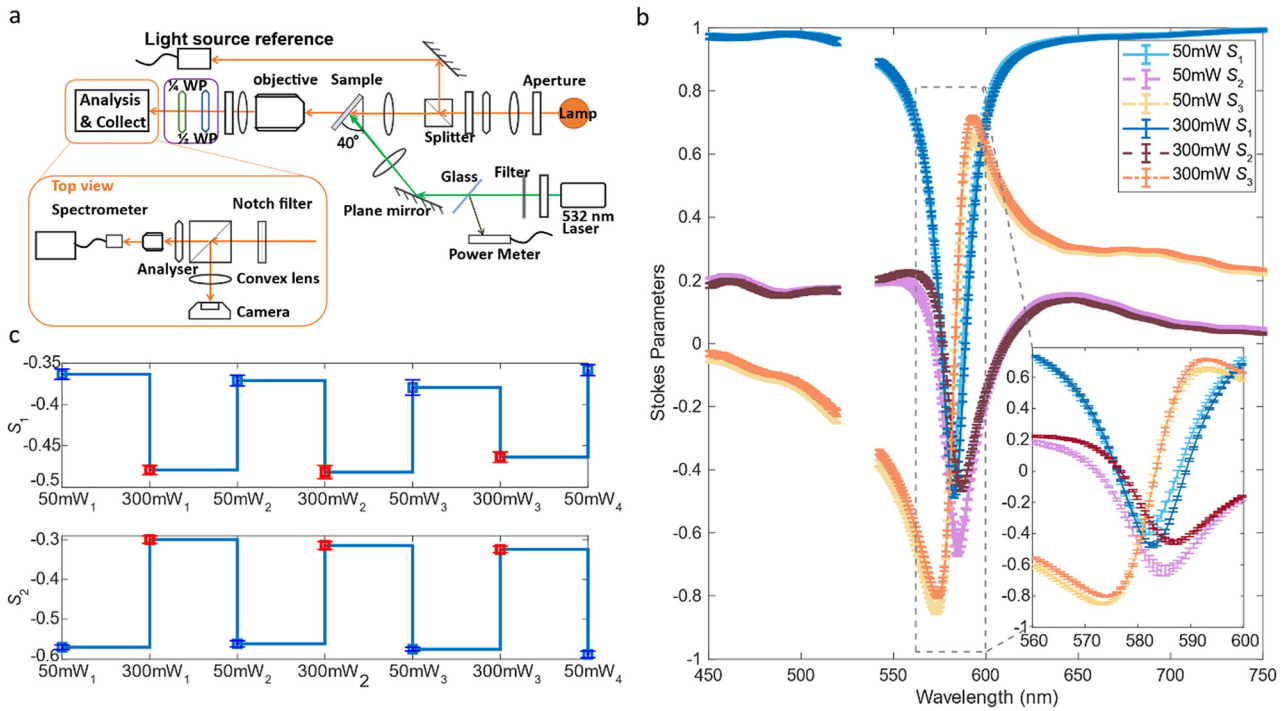

FIG. 2. (a) The schematics of the measurement setup. (b) Spectral dependence of the Stokes parameters with indicated standard deviation at low (50 mW) and high (300 mW) heating laser power. The inset shows an enlarged view of the dashed area. (c) S_1 and S_2 Stokes parameters measured over several power switch cycles for a probe wavelength of 582 nm.

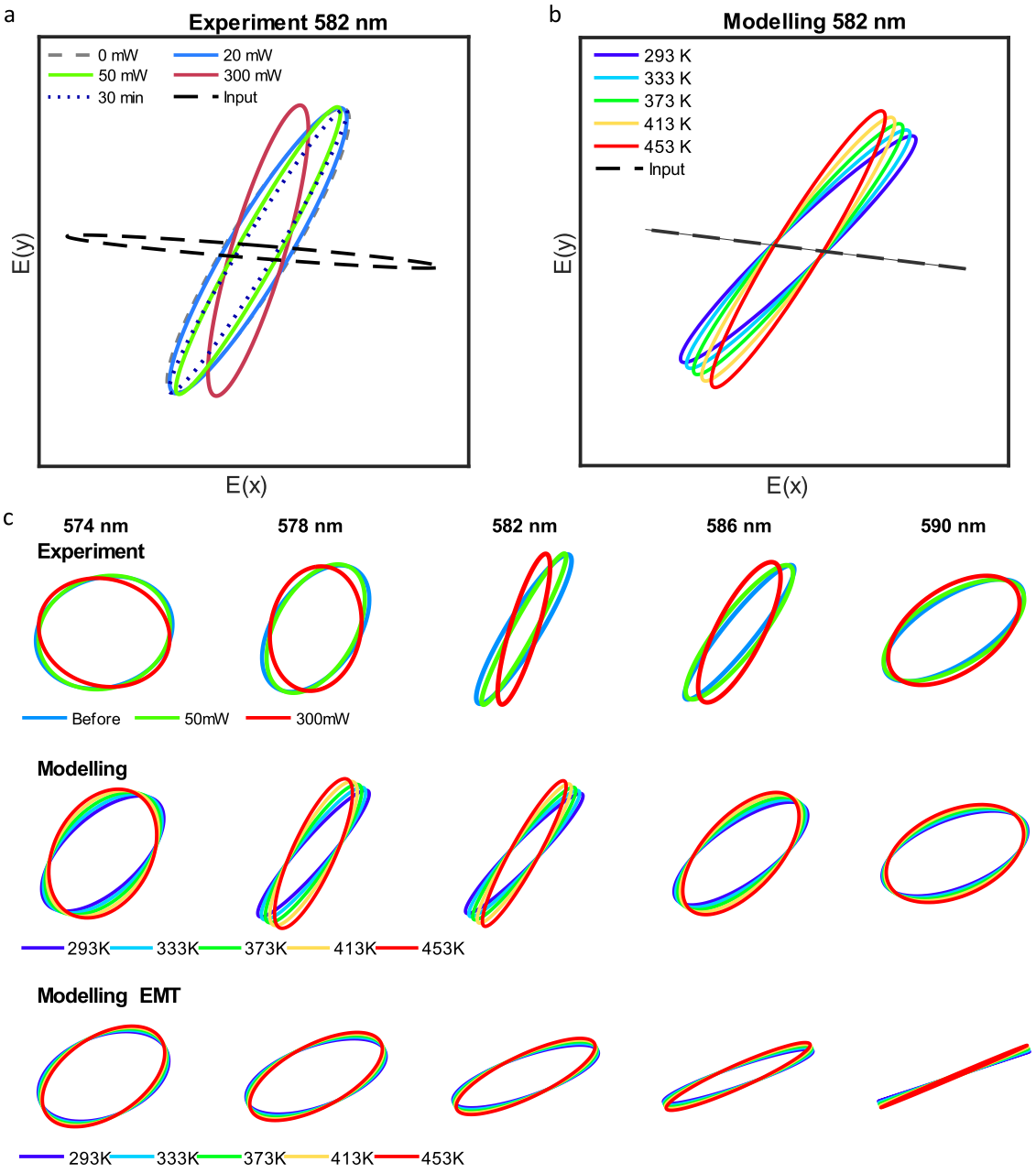

FIG. 3. (a) The change in the polarization state of the transmitted light measured at a wavelength of 582 nm at various heating conditions (30 min label denotes the measurements after the corresponding cooling time). (b) Corresponding ellipses obtained using numerical modeling for various sample temperatures. (c) Temperature-induced modification of the polarization states at various probe wavelengths in the ENZ spectral range extracted from the experiment, numerical modeling (nonlocal case) and local EMT modeling (local case).

assumption of the temperature increase of around 100 K. Modification of the polarization ellipses at various wavelengths in the ENZ spectral range shows similar trends in the temperature dependence [Fig. 3(c)]. Along with the rotation, a change in ellipticity of the polarization ellipse is observed, particularly pronounced in the ENZ regime. Contrary to previous polarization switching demonstrated in a high-peak-power pulsed regime,[46] the sensitivity of the nonlocal nanorod metamaterial implemented in the presented approach is much higher, which allows to achieve polarization control not through the nonlinear optical effects but through the temperature dependence of gold permittivity via heating/cooling.

For comparison, the simulations based on the local EMT description were employed to examine the polarization changes in the local approximation. The same metamaterial parameters and material permittivity settings were used. For identical temperature variations, smaller modifications of the polarization state were observed compared to the nonlocal case, indicating the important role of nonlocality in the polarization changes observed before in the case of transmitted intensity.[20]

In conclusion, we have demonstrated optically-induced thermal control of the polarization state of light transmitted through a plasmonic nanorod metamaterial with a nonlocal response. With the temperature increase, the Stokes parameters describing polarization of the transmitted light experience substantial changes of more than 20%, particularly in the ENZ spectral region, where the influence of nonlocality on the optical properties is strongest. This leads to the controlled rotation of the polarization ellipse by over 10°, accompanied by the change of its ellipticity by almost 7%. The effect is related to the thermal change of the permittivity of gold, resulting in different modification of the propagation of the ordinary and extraordinary waves in the metamaterial. The performed numerical simulations confirm that the observed modulation of the polarization state can be induced by the increase in the metamaterial temperature by only ∼100–150 K. The observed thermal effect is important for fine tuning of polarization of the optical beams using heat or optically-induced temperature changes in the nanorod metamaterial, or, in reverse, for temperature sensing by optical means.

This work was supported by the ERC iCOMM project (No. 789340) and the UK EPSRC Project No. EP/W017075/1.

AUTHOR DECLARATIONS

Conflict of Interest

The authors have no conflicts to disclose.

Author Contributions

Jingyi Wu: Conceptualization (equal); Formal analysis (equal); Software (equal); Writing – original draft (equal); Writing – review & editing (equal). **Anton Bykov:** Conceptualization (supporting); Formal analysis (supporting); Methodology (equal); Writing – review & editing (equal). **Alexey V. Krasavin:** Formal analysis (equal); Methodology (equal); Software (equal); Writing – original draft (equal); Writing – review & editing (equal). **Mazhar Ejaz Nasir:** Methodology (supporting); Resources (equal). **Anatoly V. Zayats:** Conceptualization (equal); Methodology (equal); Resources (equal); Writing – review & editing (equal).

DATA AVAILABILITY

The data that support the findings of this study are available from the corresponding author upon reasonable request.

REFERENCES

[1]J. Valentine, S. Zhang, T. Zentgraf, E. Ulin-Avila, D. A. Genov, G. Bartal, and X. Zhang, Nature **455**, 376 (2008).
[2]D. Lu, J. J. Kan, E. E. Fullerton, and Z. Liu, Nat. Nanotechnol. **9**, 48 (2014).
[3]N. Fang, H. Lee, C. Sun, and X. Zhang, Science **308**, 534 (2005).
[4]P. Wang, A. V. Krasavin, L. Liu, Y. Jiang, Z. Li, X. Guo, L. Tong, and A. V. Zayats, Chem. Rev. **122**, 15031 (2022).
[5]T. Cui, B. Bai, and H.-B. Sun, Adv. Funct. Mater. **29**, 1806692 (2019).
[6]S. Abdollahramezani, O. Hemmatyar, H. Taghinejad, A. Krasnok, Y. Kiarashinejad, M. Zandehshahvar, A. Alù, and A. Adibi, Nanophotonics **9**, 1189 (2020).
[7]G. A. Wurtz, R. Pollard, W. Hendren, G. P. Wiederrecht, D. J. Gosztola, V. A. Podolskiy, and A. V. Zayats, Nat. Nanotechnol. **6**, 107 (2011).
[8]N. I. Zheludev and Y. S. Kivshar, Nat. Mater. **11**, 917 (2012).
[9]G. Kafaie Shirmanesh, R. Sokhoyan, R. A. Pala, and H. A. Atwater, Nano Lett. **18**, 2957 (2018).
[10]J. Guan, J. Hu, Y. Wang, M. J. H. Tan, G. C. Schatz, and T. W. Odom, Nat. Nanotechnol. **18**, 514 (2023).
[11]D. J. Roth, A. V. Krasavin, A. Wade, W. Dickson, A. Murphy, S. Kéna-Cohen, R. Pollard, G. A. Wurtz, D. Richards, S. A. Maier, and A. V. Zayats, ACS Photonics **4**, 2513 (2017).
[12]Y. Guo, W. Newman, C. L. Cortes, Z. Jacob, and P. A. Belov, Adv. OptoElectronics **2012**, 452502.
[13]G. Marino, P. Segovia, A. V. Krasavin, P. Ginzburg, N. Olivier, G. A. Wurtz, and A. V. Zayats, Laser Photonics Rev. **12**, 1700189 (2018).
[14]M. Lapine, I. V. Shadrivov, and Y. S. Kivshar, Rev. Mod. Phys. **86**, 1093 (2014).
[15]P. Segovia, G. Marino, A. V. Krasavin, N. Olivier, G. A. Wurtz, P. A. Belov, P. Ginzburg, and A. V. Zayats, Opt. Express **23**, 30730 (2015).
[16]P. Wang, A. V. Krasavin, M. E. Nasir, W. Dickson, and A. V. Zayats, Nat. Nanotechnol. **13**, 159 (2018).
[17]Y. Liang, K. Koshelev, F. Zhang, H. Lin, S. Lin, J. Wu, B. Jia, and Y. Kivshar, Nano Lett. **20**, 6351 (2020).
[18]Y. Liang, H. Lin, K. Koshelev, F. Zhang, Y. Yang, J. Wu, Y. Kivshar, and B. Jia, Nano Lett. **21**, 1090 (2021).
[19]A. V. Kabashin, P. Evans, S. Pastkovsky, W. Hendren, G. A. Wurtz, R. Atkinson, R. Pollard, V. A. Podolskiy, and A. V. Zayats, Nat. Mater. **8**, 867 (2009).
[20]R. J. Pollard, A. Murphy, W. R. Hendren, P. R. Evans, R. Atkinson, G. A. Wurtz, A. V. Zayats, and V. A. Podolskiy, Phys. Rev. Lett. **102**, 127405 (2009).
[21]B. M. Wells, A. V. Zayats, and V. A. Podolskiy, Phys. Rev. B **89**, 035111 (2014).
[22]P. Ginzburg, D. J. Roth, M. E. Nasir, P. Segovia, A. V. Krasavin, J. Levitt, L. M. Hirvonen, B. Wells, K. Suhling, D. Richards, V. A. Podolskiy, and A. V. Zayats, Light: Sci. Appl. **6**, e16273 (2016).
[23]A. A. Orlov, P. M. Voroshilov, P. A. Belov, and Y. S. Kivshar, Phys. Rev. B **84**, 45424 (2011).
[24]J.-S. G. Bouillard, W. Dickson, D. P. O'Connor, G. A. Wurtz, and A. V. Zayats, Nano Lett. **12**, 1561 (2012).
[25]L. H. Nicholls, F. J. Rodríguez-Fortuño, M. E. Nasir, R. M. Córdova-Castro, N. Olivier, G. A. Wurtz, and A. V. Zayats, Nat. Photonics **11**, 628 (2017).
[26]P. Ginzburg, F. J. Rodríguez Fortuño, G. A. Wurtz, W. Dickson, A. Murphy, F. Morgan, R. J. Pollard, I. Iorsh, A. Atrashchenko, P. A. Belov, Y. S. Kivshar, A. Nevet, G. Ankonina, M. Orenstein, and A. V. Zayats, Opt. Express **21**, 14907 (2013).
[27]L. H. Nicholls, T. Stefaniuk, M. E. Nasir, F. J. Rodríguez-Fortuño, G. A. Wurtz, and A. V. Zayats, Nat. Commun. **10**, 2967 (2019).
[28]T. Stefaniuk, L. H. Nicholls, R. M. Córdova-Castro, M. E. Nasir, and A. V. Zayats, Adv. Mater. **35**, e2107023 (2023).
[29]A. V. Krasavin, P. Wang, M. E. Nasir, Y. Jiang, and A. V. Zayats, Nanophotonics **9**, 427 (2020).
[30]P. Evans, W. R. Hendren, R. Atkinson, G. A. Wurtz, W. Dickson, A. V. Zayats, and R. J. Pollard, Nanotechnology **17**, 5746 (2006).
[31]R. Boidin, T. Halenkovič, V. Nazabal, L. Beneš, and P. Němec, Ceram. Int. **42**, 1177 (2016).
[32]L. V. Rodríguez-de Marcos, J. I. Larruquert, J. A. Méndez, and J. A. Aznárez, Opt. Mater. Express **6**, 3622 (2016).
[33]I. H. Malitson, J. Opt. Soc. Am. **55**, 1205 (1965).
[34]C. R. Pichard, C. R. Tellier, and A. J. Tosser, Phys. Status Solidi B **99**, 353 (1980).
[35]R. Rosei, Phys. Rev. B **10**, 474 (1974).

[36]M. Guerrisi, R. Rosei, and P. Winsemius, Phys. Rev. B **12**, 557 (1975).
[37]F. Masia, W. Langbein, and P. Borri, Phys. Rev. B **85**, 235403 (2012).
[38]A. Zilli, W. Langbein, and P. Borri, ACS Photonics **6**, 2149 (2019).
[39]D. Y. Fedyanin, A. V. Krasavin, A. V. Arsenin, and A. V. Zayats, Nano Lett. **12**, 2459 (2012).
[40]D. Gall, J. Appl. Phys. **119**, 85101 (2016).
[41]P. B. Johnson and R. W. Christy, Phys. Rev. B **6**, 4370 (1972).
[42]T. Heilpern, M. Manjare, A. O. Govorov, G. P. Wiederrecht, S. K. Gray, and H. Harutyunyan, Nat. Commun. **9**, 1853 (2018).
[43]F. Castro and B. Nabet, J. Franklin Inst. **336**, 53 (1999).
[44]W. E. Lawrence, Phys. Rev. B **13**, 5316 (1976).
[45]R. T. Beach and R. W. Christy, Phys. Rev. B **16**, 5277 (1977).
[46]Y. Yang, K. Kelley, E. Sachet, S. Campione, T. S. Luk, J.-P. Maria, M. B. Sinclair, and I. Brener, Nat. Photonics **11**, 390 (2017).